Enzymatic Reactions

Real-Time NMR Monitoring of Spatially Segregated Enzymatic Reactions in Multilayered Hydrogel Assemblies**

Nurdiana Nordin[+], Lorenzo Bordonali[+], Hossein Davoodi, Novindi Dwi Ratnawati, Gudrun Gygli, Jan G. Korvink, Vlad Badilita,* and Neil MacKinnon*

Abstract: Compartmentalized chemical reactions at the micro-scale are important in biotechnology, yet monitoring the molecular content at these small scales is challenging. To address this challenge, we integrate a compact, reconfigurable reaction cell featuring electrochemical functionality with high-resolution NMR spectroscopy. We demonstrate the operation of this system by monitoring the activity of enzymes immobilized in chemically distinct layers within a multi-layered chitosan hydrogel assembly. As a benchmark, we observed the parallel activities of urease (Urs), catalase (Cat), and glucose oxidase (GOx) by monitoring reagent and product concentrations in real-time. Simultaneous monitoring of an independent enzymatic process (Urs) together with a cooperative process (GOx + Cat) was achieved, with chemical conversion modulation of the GOx + Cat process demonstrated by varying the order in which the hydrogel was assembled.

Introduction

Reproducing metabolic reactions in a controlled space that mimics the native micro-environmental conditions inside biological matter is an endeavour that can have important repercussions on bio-medical applications.[1] Spatial and temporal control over the processes that regulate metabolic activity allows to fine-tune the dynamics underlying the metabolic reaction cascade, thereby enabling researchers to engineer i) models that imitate biological environments at various spatial scales (i.e. extra- and intracellular spaces) and ii) metabolic systems with an optimized spatial arrangement of specific catalysts for a targeted application (e.g. bio-waste management, bio-production). From a medical perspective, several diagnostic platforms have been developed to inspect biomolecular abundance of metabolites with high sensitiv-

ity,[2] allowing early detection of diseases[3] and providing valuable insights into system-level[4] chemistry.

Highly hydrated polymer networks (hydrogels) are commonly used to mimic and interface with biological spaces, and their sophistication continues to evolve to keep pace with the desired performance in drug delivery, tissue engineering, and biosensing applications.[5–8] There are numerous possibilities to generate hydrogels and their composites, and one attractive route to achieve localized hydrogels in both space and time is to utilize the stimuli-responsive hydrogel sub-class. In this class, the sol-gel transition can be controlled and triggered by applying an appropriate signal; in some cases, the sol-gel transition is reversible making the system attractive, for example, in biosensing applications where the hydrogel is resettable dependent on the sensing demands. Electrochemical-based fabrication of chitosan hydrogels is one example to achieve hydrogel assembly with high spatio-temporal precision.[9,10] Chitosan is an attractive material given its properties of biocompatibility, reversible gelation, and amenability to chemical functionalization.[11–14] In addition, electrodeposition is relatively uncomplicated, requiring a two electrode system in contact with a chitosan solution to generate a local increase in pH with an applied current, thereby causing local deposition of the chitosan hydrogel. This has been exploited for (bio)sensing[15–18] and controlled release[19,20] applications.

Since the deposition process is controlled by an electrical signal, the architecture of the hydrogel can be varied simply by modulating the trigger signal. This results in a multilayered structure,[21,22] which can be used to encode information[23] or to generate cell bioreactors.[24] Taking advantage of the ability to chemically functionalize chitosan prior to deposition, our group has demonstrated that each layer can be additionally assigned a unique chemical identity.[25] In this way, complex hydrogel structures can be assembled with programmable

---

[*] N. Nordin,[+] L. Bordonali,[+] H. Davoodi, N. D. Ratnawati,
    J. G. Korvink, V. Badilita, N. MacKinnon
    Institute of Microstructure Technology
    Karlsruhe Institute of Technology
    Eggenstein-Leopoldshafen (Germany)
    E-mail: vlad.badilita@kit.edu
            neil.mackinnon@kit.edu

    N. Nordin[+]
    Department of Chemistry, Faculty of Science, University of Malaya
    Kuala Lumpur (Malaysia)

    G. Gygli
    Institute of Biological Interfaces-1, Karlsruhe Institute of Technology
    Eggenstein-Leopoldshafen (Germany)

[+] These authors contributed equally to this work.

spatial separation of chemical function. Given that control of layer thickness can be on the order of micrometers, there is potential to leverage this technology in the direction of replicating the spatial localization of metabolic and functional elements within tissues. At these length scales, microfluidic methods are critical for the handling and management of the resultant small sample volumes.

Nuclear magnetic resonance (NMR) spectroscopy in combination with microfluidics has been identified as a powerful analytical method when both small sample management and in situ investigation of metabolic activity are required.[26–28] NMR is non-invasive and reports on the dynamics of a (bio)chemical reaction with high resolution along both time and frequency (i.e. chemical) dimensions. In the context of NMR monitoring of localized metabolic activity, the challenge is to integrate additional functionalities into the detection space without degrading the SNR of the NMR signal and without perturbing the homogeneity of the local magnetic environment necessary for high quality NMR spectra. Our group has previously reported that integration of hardware elements for simple electrochemical manipulations inside the active region of an NMR micro-detector is possible, without compromising the overall quality of the recorded spectrum.[29]

In this report, we describe functional monitoring of spatially localized enzymes within a microfluidic device by a micro-NMR system. By electrodeposition, a chitosan hydrogel was co-localized with an electrode while the catalytic potential perpendicular to the electrode surface was controlled by sequential deposition of chitosan layers modified with different enzymes. Urease (Urs), glucose oxidase (GOx), and catalase (Cat) were selected for a three-layer system, representing independent conversion of urea (to ammonia via Urs) and glucose (to gluconic acid via GOx) and a coupled enzymatic reaction (peroxide generated by GOx to water via Cat). In the microfluidic device, conversion of approximately 3 µmol of urea and 0.3 µmol of glucose by a multi-functional chitosan hydrogel was measured, demonstrating simultaneous monitoring of multiple biocatalytic reactions within a hydrogel matrix.

Results and Discussion

A custom NMR probe head insert, compatible with a commercial Bruker Micro5 microimaging NMR probe, was designed and fabricated to enable NMR monitoring of an in situ electrodeposition experiment (Figure 1).
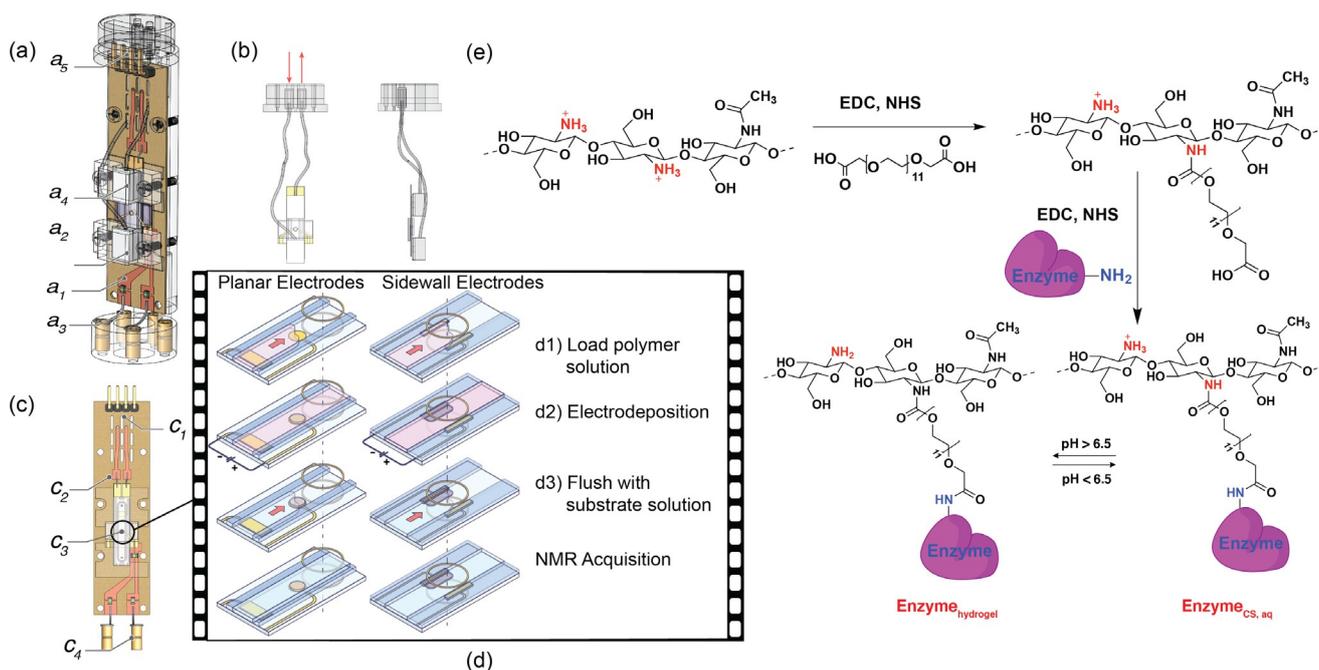
Figure 1. Experimental setup for in situ electrodeposition of pre- and post- modified chitosan inside the microfluidic chip. a) overview of the NMR probe head insert with the main elements: a1) PCB hosting RF tracks, tuning and matching fixed capacitors, the electrodeposition tracks and the NMR microcoil, a2) the microfluidic insert mounted inside the Helmholtz microcoil, a3) insert base with RF female connectors, a4) microfluidic connectors and connectors clamps, a5) topside connector supporting both electrical and fluidic connections to the outside. b) Fluidic components, left side view and top view. c) Highlighted electrical components: c1) electrodeposition lines and PCB header connector, c2) tin-plated copper connections between PCB and microfluidic insert, c3) microcoil NMR detector, c4) ^{1}H NMR RF lines. d) Illustration of the in situ electrodeposition process (planar and side-wall electrode configurations): d1) loading the microfluidic channel with the polymer solution, d2) initiate electrodeposition, d3) rinsing with a buffer and/or loading the channel with a reagent solution prior to the NMR experiment. The vertical dashed line indicates the position of the NMR detection volume defined by the NMR detector (wire loops above and below the fluidic insert). e) The general chemical process used to functionalize chitosan with the enzymes. After functionalization, chitosan retains the ability to undergo a sol–gel transition.

The NMR detector used in this work was a Helmholtz pair with a 1.2 mm diameter and 600 μm separation between the two windings.[27] The microcoil was mounted on top of a PCB (printed circuit board), hosting both the ^{1}H NMR channel tracks interfaced to the NMR probe head, and chitosan electrodeposition tracks connected to a power source outside of the magnet using a PCB pinheader (Figure 1a). The support structure of the probe insert was fabricated in PMMA.

Two variations of an application-specific sample insert[27] were considered for the in situ electrochemistry experiment. For the first variation, the electrode pair was planar and was patterned on the bottom surface of the microfluidic channel (planar configuration): one round working electrode with a 1.5 mm diameter (total area 1.76 mm^2) and a rectangular counter electrode 1.5 mm × 2 mm. In this case the microfluidic channel had a total sample capacity of 3.2 μL. In this configuration, the electrode, and therefore assembled hydrogel, was placed slightly upstream of the NMR detection volume in order to minimize electrode-related NMR artifacts.

For the second variation, the electrodes were placed along the walls of a 1.1 mm-wide fluidic channel (sidewall configuration) so that, when inserted into the NMR detector, the electrodes were at the periphery of the Helmholtz coil. In this configuration, the area of both the working and the counter electrodes is 0.43 mm^2 and the total sample capacity is 2.6 μL. It is noted that this configuration places the hydrogel within the NMR detection volume. Details regarding the design and fabrication of the electrodeposition sample inserts, as well as a discussion about the compatibility with the Helmholtz NMR detector, have been reported elsewhere.[29]

Electrical connection to the host PCB electrodeposition lines was done by soldering tin-plated copper wire to the gold pads of the microfluidic insert (Figure 1c). Fluidic contact with the insert was achieved by interfacing soft silicon tubing to the glass insert inlet and outlet ports using custom connectors (machined Teflon) and soft PDMS pads (Figure 1b). The silicon tubing was fed to the top of the insert assembly and connected to fluidic lines outside of the magnet bore.

After assembly and installation of the probe, a typical NMR experiment proceeded as follows (Figure 1c): 1) a solution containing chitosan functionalized with the desired enzyme was flushed through the system to fill the microfluidic insert; 2) a DC current was applied to the pair of electrodes for 15 min to perform hydrogel electrodeposition; 3) a rinsing solution (buffered at pH 7) was gently flushed through to stabilize the hydrogel; 4) a solution containing the desired substrates was flushed through the system. Depending on the particular experiment, steps 1–3 were repeated to build a layered hydrogel before flushing the hydrogel assembly with substrate solution. After step 4) the probe was inserted into the magnet bore to begin the NMR measurement routine.

NMR spectra were collected on a Bruker AVANCE III system operating at a [1]H Larmor frequency of 500.13 MHz. A series of spectra were collected, each acquisition requiring 9 min with a 15 min delay between subsequent acquisitions, so that initiation of acquisitions were separated by 24 min in time. The microfluidic insert placement was such that the working electrode in the planar configuration was not within the NMR detector (i.e. the hydrogel was not in the detector), while the electrodes were placed at the periphery of the detector in the sidewall configuration (i.e. the hydrogel was in the detector). Schematic representations of these configurations are given in Figure 1d.

In this work, urease (Urs: jack bean, EC 3.5.1.5), catalase (Cat: bovine liver, EC 1.11.1.6), and glucose oxidase (GOx: from *Aspergillus niger*, EC 1.1.3.4) were chosen as model enzymes to verify that i) covalent enzyme attachment to chitosan does not inhibit their catalytic ability; ii) catalytic activity is maintained when deposited as a multilayered hydrogel; iii) microfluidic NMR can be used to monitor catalytic turnover. Both Urs and GOx have been observed to be catalytically active while integrated within a hydrogel.[30]

The enzymes were connected to chitosan using a difunctional polyethylene glycol (PEG) linker and NHS/EDC coupling chemistry (schematic in Figure 1e). It was observed previously that PEG retains molecular mobility when tethered to chitosan,[29] and therefore it was anticipated this mobility would be useful in maintaining enzyme function. Coupling efficiency to the PEG-modified chitosan was estimated by UV/Vis spectroscopic analysis of the reaction solution after precipitation of the hydrogel (Figure S2). The coupling efficiencies observed were 41% for Urs and 35% for GOx.

To determine to what extend the enzymes (Urs, Cat and GOx) retained their activity in the chitosan hydrogel, the following experiments were performed: i) determination of enzyme activity in solution (Urs$_{aq}$, Cat$_{aq}$, and GOx$_{aq}$), ii) activity of the chitosan coupled enzymes in solution (Urs$_{CS,aq}$, Cat$_{CS,aq}$, and GOx$_{CS,aq}$), and iii) the activity of the enzymes after hydrogel electrodeposition (Urs$_{hydrogel}$ and Cat-GOx$_{hydrogel}$). Please note, multilayered hydrogels will be denoted by listing the enzymes in order of their hydrogel deposition layer, Layer1-Layer2-Layer2$_{hydrogel}$.

The results for Urs are presented in Figure 2. The NMR results for Urs$_{aq}$ and Urs$_{CS,aq}$ are plotted in Figure 2a (top, filled and open symbols, respectively, spectra in Figure S9). The results indicate that, indeed, Urs maintained activity after covalent attachment to chitosan. A slight increase in the initial rate is observed for Urs$_{CS,aq}$ compared to Urs$_{aq}$, which we attribute to an increased buffering capacity in the presence of chitosan. In the absence of CS, the pH was observed to increase from 5.5 to 9 at the end of the reaction, while the presence of CS controlled the pH such that it increased from 5.5 to 6.5 (Figure S5a). At elevated pH, Urs activity is expected to be limited, with reports noting that Urs maintains activity from below pH 3 to 7.5.[31,32] Importantly, after electrodeposition of a single layer Urs$_{hydrogel}$, Urs activity remained unchanged compared to the Urs$_{CS,aq}$ case (Figure 2a, bottom).

The results for the GOx and Cat pair are presented in Figure 3. In this case, both reactant consumption (glucose) and product formation (gluconic acid) could be followed by NMR spectroscopy. For Cat$_{aq}$ and GOx$_{aq}$, the results are plotted in Figure 3a (top, filled symbols). To perform the CS-coupled experiments, two polymer solutions were prepared: GOx$_{CS,aq}$ and Cat$_{CS,aq}$. The two polymer solutions were mixed
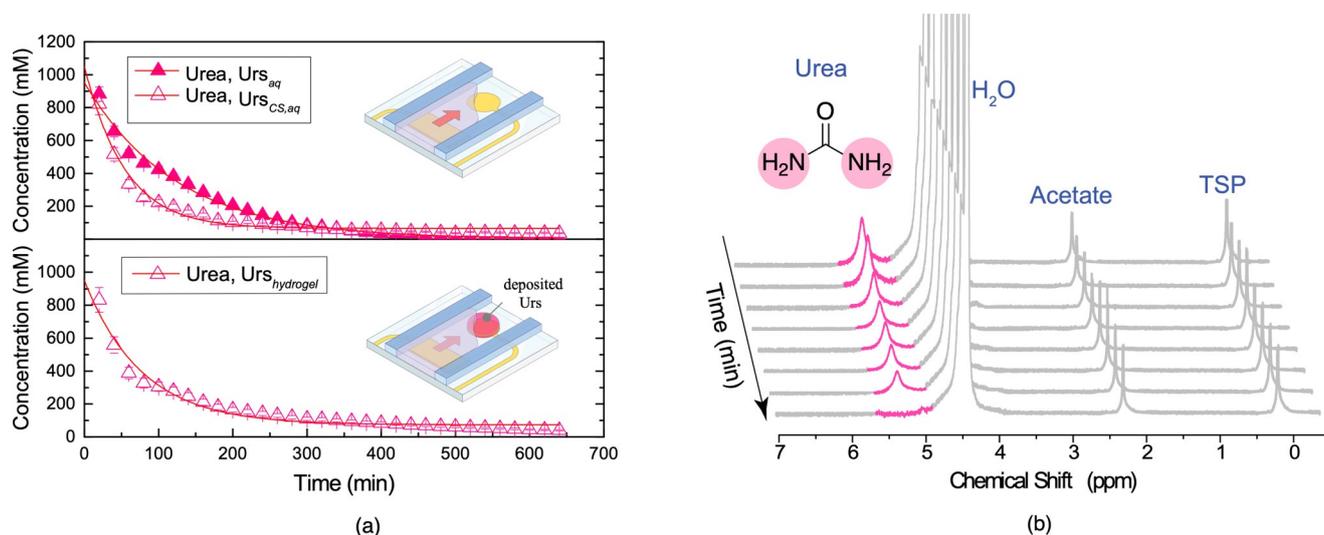
Figure 2. ^{1}H NMR monitoring or Urs activity. a) Extracted urea concentration in the presence of: top: Urs$_{aq}$ (filled symbols) and Urs$_{CS,aq}$ (open symbols); bottom: Urs$_{hydrogel}$. b) Representative ^{1}H NMR spectra obtained for Urs$_{hydrogel}$. The hydrolysis of urea (highlighted in pink, 5.8 ppm) is shown as a function of time. The urea concentration was calculated using the internal standard (TSP, 50 mM). The fits to the data were obtained using Equations S1 and S2, apparent kinetic parameters summarized in Table S1. NMR spectra for Urs$_{aq}$ and Urs$_{CS,aq}$ are plotted in Figure S9. The electrodeposition electrode was placed slightly upstream of the NMR detector (Figure 1d).
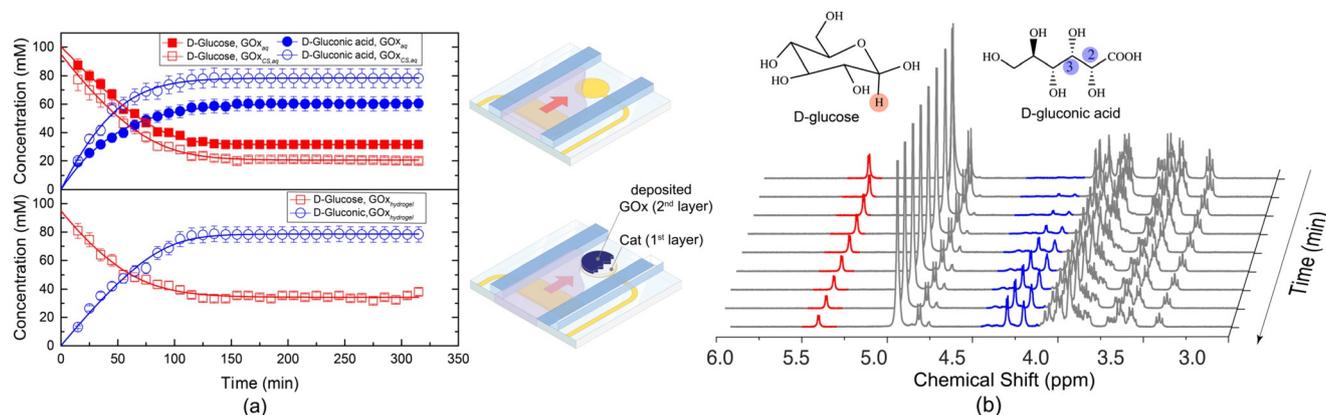
Figure 3. ^{1}H NMR monitoring or GOx + Cat activity. a) Extracted glucose and gluconic acid concentrations in the presence of: top: GOx$_{aq}$ + Cat$_{aq}$ (filled)* and GOx$_{CS,aq}$ + Cat$_{CS,aq}$ (open); bottom: electrodeposited dual-layer Cat-GOx$_{hydrogel}$, and b) representative ^{1}H NMR spectra obtained for the electrodeposited Cat-GOx$_{hydrogel}$. Concentrations were determined using the internal reference (TSP, 50 mM). The depletion of glucose (marked red, 5.8 ppm) upon conversion to gluconic acid (marked blue, 4–4.2 ppm) is shown as a function of time. Best-fit curves obtained using Equations S1 and S2 are plotted, apparent kinetic parameters are summarized in Table S1. NMR spectra for GOx$_{aq}$ + Cat$_{aq}$ and GOx$_{CS,aq}$ + Cat$_{CS,aq}$ are plotted in Figure S10. *GOx experiments were always performed using GOx:Cat in a 4:1 ratio. The electrode was placed slightly upstream of the NMR detector (Figure 1d).

to maintain the 4:1 ratio of GOx:Cat and maintain the expected concentration of GOx at 4 mg mL^{-1} (actual [GOx] ca. 1.4 mg mL^{-1} after accounting for coupling yield). NMR measurement results are presented in Figure 3a (top, open symbols, spectra in Figure S10). As in the case of Urs, GOx retains its activity after coupling to chitosan. The resulting kinetics are very similar in solution and when covalently attached to the polymer; however, it is noted that glucose does not undergo complete conversion. A possible explanation for the incomplete substrate conversion is an oxygen deficiency. In the presence of catalase, 0.5 mol of oxygen is consumed for every mol of glucose. Since the reaction volume was only 3.2 μL and the materials used to fabricate the device

restrict oxygen diffusion into the solution, oxygen could have become the limiting reagent as the reaction progressed. This is supported by control experiments performed in standard 5 mm NMR tubes, where the sample volume is 500 μL and a large gas headspace is available in the NMR tube. Every other parameter held constant, glucose was observed to be fully consumed under these conditions (Figure S13). This highlights the importance of considering oxygen perfusion in microfluidic devices in cases where it participates in the process.[33]

As was observed with Urs$_{hydrogel}$, glucose conversion to gluconic acid could be observed in the electrodeposited Cat-GOx$_{hydrogel}$ (Figure 3a, bottom) as has been reported,[34] with
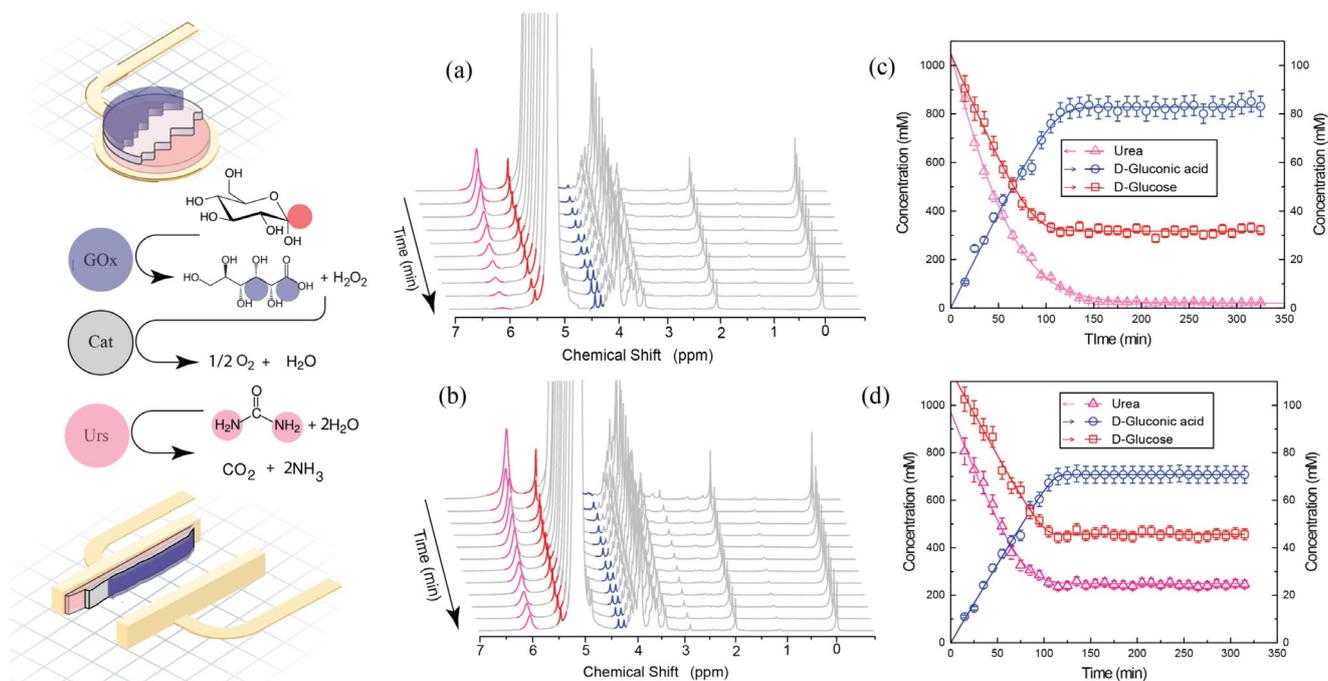
Figure 4. Left: the enzymatic reactions performed with Urs-Cat-GOx$_{hydrogel}$. Position of NMR- integrated hydrogens are highlighted in red (glucose), blue (gluconic acid), and pink (urea). The arrangement of the hydrogel assembly is displayed for the case of a planar electrode (top) and a sidewall electrode (bottom). Gel layers have been colored in blue for GOx$_{hydrogel}$, gray for Cat$_{hydrogel}$, and pink for Urs$_{hydrogel}$. a),b) Representative ^{1}H NMR time series of Urs and GOx enzymatic reactions. Experiments were performed on a) a planar electrode and b) a sidewall electrode. Signals are colored according to the color coding on the left (urea at 5.8 ppm, the glucose signal at 5.3 ppm, the gluconic acid signal at 4.2 ppm). c),d) Concentration time series of reactants and products extracted from NMR spectra in (a) and (b), by integrating NMR signals in the highlighted regions. Left axis: concentration of urea; right axis: concentrations of both glucose and gluconic acid. Solid lines are best-fit curves to the Michaelis–Menten kinetic model (Equations S1 and S2). Apparent kinetic parameters are summarized in Table S3. Reproducibility is presented in Figure S8. Data for the enzyme mixture in solution, free and CS-coupled, are presented in Figures S11 and S12.

the kinetics essentially identical to the GOx$_{CS,aq}$ + Cat$_{CS,aq}$ case. A key difference compared to the Urs$_{hydrogel}$ was that a two layer Cat-GOx$_{hydrogel}$ was generated for this experiment.

Comparing the Enzyme$_{CS,aq}$ and Enzyme$_{hydrogel}$ assembly cases, catalytic performance was observed to be independent of chitosan existing in either the solution or hydrogel states. For a discussion on the kinetics analysis, please refer to the Supporting Information.

To further extend the catalytic functionality of the multi-layer hydrogel assembly beyond the GOx + Cat cascade, a three layer hydrogel was deposited with the composition Urs-Cat-GOx$_{hydrogel}$ (Figure 4a). This multiplexed system was prepared using two different electrode geometries, taking advantage of our recent investigation into optimizing electrode placement with respect to the NMR detection volume.[29] The planar geometry, as was used for Urs$_{hydrogel}$ and Cat-GOx$_{hydrogel}$ examples, was used to place the catalytic hydrogel assembly slightly upstream (i.e. outside) of the NMR detector. The side-wall electrode geometry, with better NMR performance, was used to place the hydrogel within the NMR detector.

The ^{1}H NMR spectra and extracted concentration profiles versus time after exposure to a 1000 mM urea and 100 mM glucose (200 mM NaAc, pH 7) solution are presented in Figure 4 for both electrode geometries.

The NMR data clearly show the ability to monitor both reactions (urea hydrolysis, glucose oxidation) simultaneously.

The substrates (urea, glucose) and product (gluconic acid) all have unique signals that can be used for quantitative determination of the catalytic processes. The extracted kinetic data is summarized in Table S3.

Figure 4 presents the activity for the Urs-Cat-GOx$_{hydrogel}$ assembly. Three additional experiments were done after permuting the hydrogel composition: Urs-GOx-Cat$_{hydrogel}$, Cat-Urs-GOx$_{hydrogel}$, GOx-Cat-Urs$_{hydrogel}$. As presented in Figure 5, the observed Urs activity was independent of programmed composition. Conversely, glucose conversion to gluconic acid was dependent on the order in which the hydrogel was assembled. Considering only Brownian diffusion, a water molecule would require approximately 3 ms to achieve a mean squared displacement of 45 μm, approximately the total thickness of the hydrogel assembly (assuming $D_{o,water} = 2.3$ μm^{2}ms^{-1}). Even if the effective viscosity increases by three orders of magnitude due to the hydrogel (which is unlikely given it is > 85% water), the time scale for transport across the hydrogel assembly is small in comparison to the NMR acquisition time. Therefore, the results for Urs in Figure 5 are not completely surprising, as urea is nearly the same size as a water molecule. Interestingly, the dependence of glucose conversion suggests that hydrogel composition can be used to tune catalytic processes as, for example, Cat-Urs-GOx$_{hydrogel}$ produced ca. 10% less gluconic acid compared to GOx-Cat-Urs$_{hydrogel}$. Parameters to consider in tuning coupled catalytic processes include varying the hydrogel thickness,
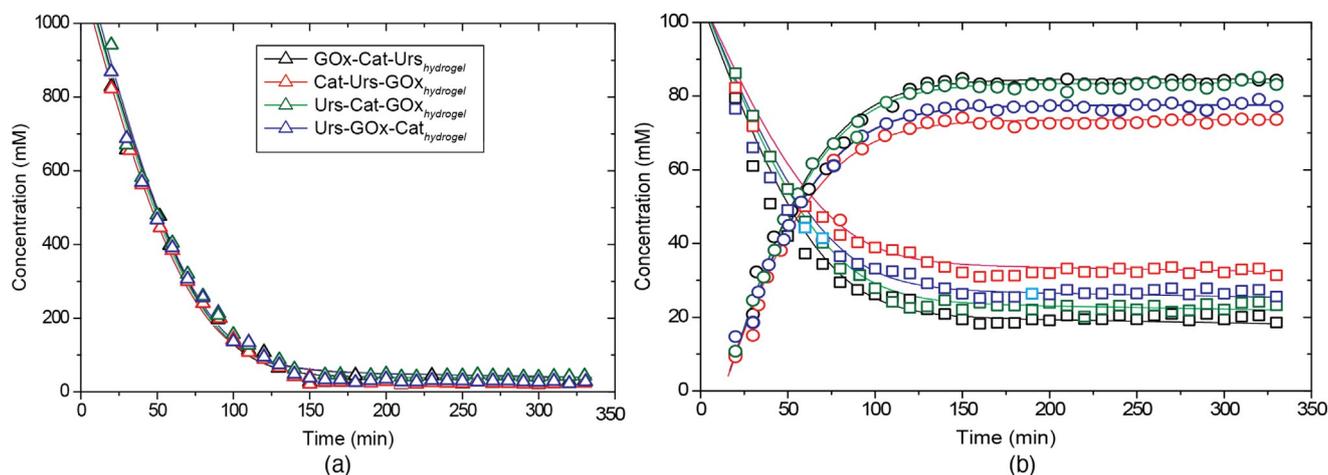
Figure 5. Comparison of enzyme activity measured for 4 different electrodeposited hydrogel assemblies. ^{1}H NMR data were collected using the planar electrode configuration. a) Urea consumption; b) glucose consumption and gluconic acid production. The legend is the same for both plots. Solid lines are best-fit curves to the Michaelis- Menten kinetic model fitting the apparent kinetic parameters (Equations S1 and S2).

introducing intermediate layers and changing the degree of cross-linking, and/ or spatially separating hydrogel assemblies on different electrodes within the same fluidic channel.

As observed in Figure 4, the new feature in the data observed in comparing the two electrode geometries was the incomplete conversion of urea in the side-wall electrode case. This is attributed to inhibition; inhibition constants for urea (substrate) and ammonium (product) are in the range 3–6.4 M and 2–118 mM,[35] within an order of magnitude of the initial urea concentrations used in these experiments (1 M). Since the total volume of Urs$_{hydrogel}$ is approximately a factor of 4 less for the side-wall configuration (Figure S6), the effective number of active Urs units will be correspondingly reduced and we speculate that the inhibitory effect of both the substrate and product was therefore stronger. Nevertheless, it was observed that activity could be monitored when placing the hydrogel within the NMR sensitive volume with minimal deleterious spectral effects (e.g. line broadening).

Conclusion

The compositionally customizable microfluidic system described in this study reveals the dynamics of multiple immobilized enzymes within an NMR detection volume. Each immobilized enzyme (Urs and GOx) performs its selective chemistry independent of the substrate solution mixture (urea and glucose), as expected. By spatially separating the functionality in the layered hydrogel assembly, new dimensions to studying enzymatic processes are envisioned, for example: i) by controlling layer thicknesses and chemical identity, mass transit between layers can be tuned; ii) multi-step chemical conversion can be designed by controlling the spatial location of the relevant catalysts; iii) more than one independent reaction cascade can be programmed into the hydrogel assembly, enabling multiplexed experiments. In this work, biological catalysis was demonstrated, and this could be extended to homogeneous and heterogeneous catalytic processes in situations where the chemistry is water based (taking

advantage of the hydrogel architecture) and the catalyst can be immobilized (chemically or physically) to distinct hydrogel layers. Cases in which the presence of one catalyst is deleterious to the function of another catalyst (e.g. by binding interference) can be additionally considered given the ease of compartmentalization enabled by the layered assembly. Sophisticated multi-functional surfaces can therefore be designed, applicable (non-exclusively) to metabolic engineering, (bio)sensing, and biomimicry investigations.

Conflict of Interest

The authors declare no conflict of interest.

[1] S. Ahmed, V. M. Chauhan, A. M. Ghaemmaghami, J. W. Aylott, *Biotechnol. Lett.* **2019**, *41*, 1–25.

[2] M. M.-C. Cheng, G. Cuda, Y. L. Bunimovich, M. Gaspari, J. R. Heath, H. D. Hill, C. A. Mirkin, J. Nijdam, R. Terracciano, T. Thundat, et al., *Curr. Opin. Chem. Biol.* **2006**, *10*, 11–19.

[3] J. D. Wulfkuhle, L. A. Liotta, E. F. Petricoin, *Nat. Rev. Cancer* **2003**, *3*, 267.

[4] L. Hood, J. R. Heath, M. E. Phelps, B. Lin, *Science* **2004**, *306*, 640–643.

[5] G. Milcovich, S. Lettieri, F. E. Antunes, B. Medronho, A. C. Fonseca, J. F. Coelho, P. Marizza, F. Perrone, R. Farra, B. Dapas, G. Grassi, M. Grassi, S. Giordani, *Adv. Colloid Interface Sci.* **2017**, *249*, 163–180.

[6] K. Wang, Y. Hao, Y. Wang, J. Chen, L. Mao, Y. Deng, J. Chen, S. Yuan, T. Zhang, J. Ren, W. Liao, *Int. J. Polym. Sci.* **2019**, *2019*, 3160732.

[7] S. C. Neves, L. Moroni, C. C. Barrias, P. L. Granja, *Trends Biotechnol.* **2020**, *38*, 292–315.

[8] S. Mondal, S. Das, A. K. Nandi, *Soft Matter* **2020**, *16*, 1404–1454.

[9] J. Li, S. Wu, E. Kim, K. Yan, H. Liu, C. Liu, H. Dong, X. Qu, X. Shi, J. Shen, W. E. Bentley, G. F. Payne, *Biofabrication* **2019**, *11*, 032002.

[10] E. R. Cross, *SN Appl. Sci.* **2020**, *2*, 397.

[11] Y. Cheng, K. M. Gray, L. David, I. Royaud, G. F. Payne, G. W. Rubloff, *Mater. Lett.* **2012**, *87*, 97–100.

[12] C. Cao, E. Kim, Y. Liu, M. Kang, J. Li, J.-J. Yin, H. Liu, X. Qu, C. Liu, W. E. Bentley, G. F. Payne, *Biomacromolecules* **2018**, *19*, 3502–3514.

[13] Y. Cheng, X. Luo, J. Betz, S. Buckhout-White, O. Bekdash, G. F. Payne, W. E. Bentley, G. W. Rubloff, *Soft Matter* **2010**, *6*, 3177–3183.

[14] C. Hao, L. Ding, X. Zhang, H. Ju, *Anal. Chem.* **2007**, *79*, 4442–4447.

[15] H. Yi, L. Wu, J. J. Sumner, J. B. Gillespie, G. F. Payne, W. E. Bentley, *Biotechnol. Bioeng.* **2003**, *83*, 646–652.

[16] X. Luo, J. Xu, Y. Du, H. Chen, *Anal. Biochem.* **2004**, *334*, 284.

[17] E. R. Mamleyev, S. Heissler, A. Nefedov, P. G. Weidler, N. Nordin, V. V. Kudryashov, K. La"nge, N. MacKinnon, S. Sharma, *NPJ Flexible Electronics* **2019**, *3*, 2.

[18] W. Shang, C. Chen, K. Lo, G. F. Payne, W. E. Bentley, *Sens. Actuators B* **2019**, *295*, 30–39.

[19] Y. Liu, K. Yan, G. Jiang, Y. Xiong, Y. Du, X. Shi, *Int. J. Polym. Sci.* **2014**, *2014*, 736898.

[20] P. Zhao, Y. Zhao, L. Xiao, H. Deng, Y. Du, Y. Chen, X. Shi, *Colloids Surf. B* **2017**, *158*, 474–479.

[21] K. Yan, Y. Liu, J. Zhang, S. O. Correa, W. Shang, C. Tsai, W. E. Bentley, J. Shen, G. Scarcelli, C. B. Raub, X. Shi, G. F. Payne, *Biomacromolecules* **2018**, *19*, 364–373.

[22] S. Wu, K. Yan, J. Li, R. N. Huynh, C. B. Raub, J. Shen, X. Shi, G. F. Payne, *React. Funct. Polym.* **2020**, *148*, 104492.

[23] K. Yan, F. Ding, W. E. Bentley, H. Deng, Y. Du, G. F. Payne, X. Shi, *Soft Matter* **2014**, *10*, 465–469.

[24] S. Ladet, K. Tahiri, A. Montembault, A. Domard, M. M. Corvol, *Biomaterials* **2011**, *32*, 5354–5364.

[25] N. Nordin, L. Bordonali, V. Badilita, N. MacKinnon, *Macromol. Biosci.* **2019**, *19*, 1800372.

[26] V. Badilita, R. C. Meier, N. Spengler, U. Wallrabe, M. Utz, J. G. Korvink, *Soft Matter* **2012**, *8*, 10583–10597.

[27] N. Spengler, J. Ho"fflin, A. Moazenzadeh, D. Mager, N. MacKinnon, V. Badilita, U. Wallrabe, J. G. Korvink, *PloS One* **2016**, *11*, e0146384.

[28] B. Wu, S. von der Ecken, I. Swyer, C. Li, A. Jenne, F. Vincent, D. Schmidig, T. Kuehn, A. Beck, F. Busse, et al., *Angew. Chem. Int. Ed.* **2019**, *58*, 15372–15376; *Angew. Chem.* **2019**, *131*, 15516–15520.

[29] H. Davoodi, N. Nordin, L. Bordonali, J. G. Korvink, N. MacKinnon, V. Badilita, *Lab Chip* **2020**, *20*, 3202–3212.

[30] Y. Ogawa, K. Ogawa, B. Wang, E. Kokufuta, *Langmuir* **2001**, *17*, 2670–2674.

[31] S. F. Howell, J. B. Sumner, *J. Biol. Chem.* **1934**, *104*, 619–626.

[32] B. Krajewska, S. Ciurli, *Plant Physiol. Biochem.* **2005**, *43*, 651–658.

[33] A. Yilmaz, M. Utz, *Lab Chip* **2016**, *16*, 2079.

[34] J. Li, D. Maniar, X. Qu, H. Liu, C. Tsao, E. Kim, W. E. Bentley, C. Liu, G. F. Payne, *Biomacromolecules* **2019**, *20*, 969–978.

[35] B. Krajewska, *J. Mol. Catal. B* **2009**, *59*, 9–21.